Bidentate pyridyl-NHC ligands: synthesis, ground and excited state properties of their iron(II) complexes and role of the fac/mer isomerism

Kévin Magra, Antonio Francés-Monerris, Cristina Cebrian, Antonio Monari, Stefan Haacke, Philippe Gros

Bidentate pyridyl-NHC ligands: synthesis, ground and excited state properties of their iron(II) complexes and role of the fac/mer isomerism

Kévin Magra,[a] Antonio Francés-Monerris,[b] Cristina Cebrián,*[a] Antonio Monari,[c,d] Stefan Haacke[e] and Philippe C. Gros[f]

Dedicated to Professor Marc Beley for his contribution to the field of Coordination and Organometallic Chemistry

[a] Dr. K. Magra, Dr. C. Cebrián
Université de Lorraine, CNRS, L2CM
57000 Metz, France
E-mail: cristina.cebrian-avila@univ-lorraine.fr
http://www.l2cm.univ-lorraine.fr/l2cm/
https://twitter.com/L2CM_UMR7053
[b] Dr. A. Francés-Monerris
Departament de Química Física, Universitat de València,
46100 Burjassot, Spain
[c] Prof. A. Monari
Université de Lorraine, CNRS, LPCT
F-54000 Nancy, France
[d] Prof. A. Monari
Université de de Paris and CNRS, Itodys
F-75006 Paris, France
[e] Prof. S. Haacke
Université de Strasbourg, CNRS, IPCMS
F-67000 Strasbourg, France
[f] Dr. P. C. Gros
Université de Lorraine, CNRS, L2CM
54000 Nancy, France

Supporting information for this article is given via a link at the end of the document.

Abstract: Iron complexes are promising candidates for the development of sustainable molecular photoactive materials as an alternative to those based on precious metals such as Ir, Pt or Ru. These compounds possess metal-ligand charge transfer (MLCT) transitions potentially of high interest for energy conversion or photocatalysis applications if the ultrafast deactivation via lower-lying metal-centred (MC) states can be impeded. Following an introduction describing the main design strategies used so far to increase the MLCT lifetimes, we review some of our latest contributions to the field regarding bidentate Fe(II) complexes comprising N-heterocyclic carbene ligands. The discussion covers all aspects from their synthesis to their characterization via photophysical, electrochemical and computational techniques. The impact of bidentate coordination together with the configuration (facial and meridional isomers) is analysed, finally highlighting the current challenges in this promising area.

1. Introduction

The development of Earth-abundant metal-based photoactive materials is a big challenge for the scientific community, gathering considerable efforts in the last few years.[1] Up to now, these materials have been mostly based on precious metals such as iridium, platinum or ruthenium due to their tuneable and long-lived excited states, luminescence and/or redox properties, finding applications in opto-electronics,[2] solar energy conversion,[3] and photocatalysis,[4] among others.

However, scarcity, cost and the sometimes non-negligible toxicity of precious metals can dramatically limit large-scale applications. For instance, ruthenium complexes are privileged sensitizers in dye-sensitized solar cells (DSSCs) as a result of their absorption, which covers a wide portion of the solar spectrum, and their fast electron injection into the semiconductor via long-lived metal-to-ligand charge transfer (MLCT) excited states.[5,6] Cheaper iron-based compounds were proposed as the ideal eco-friendly alternatives to toxic Ru^{II}-based dyes.[7,8] However, the ^{1,3}MLCT states in Fe^{II}-polypyridyl complexes undergo ultrafast deactivation via the population of the low lying metal-centred (MC) states,[9–11] from which electron transfer reactions to the semiconductor[7,12,13] have not been proven so far.[14]

Consequently, the development of iron-based excitonic devices is conditioned by the availability of compounds with long-lived MLCT states. Recently, the use of *N*-heterocyclic carbenes (NHC) ligands has brought a real breakthrough in the race for excited-state lifetime improvement of organometallic iron complexes. In particular, the use of tridentate pyridyldicarbene ligands allowed the achievement of a remarkable ^{3}MLCT lifetime of 9 ps for complex **1a** (Figure 1).[15] The strong σ-donor character of these ligands promotes a higher ligand field splitting of the iron d orbitals,[16] resulting in a destabilisation of the MC states over the MLCT manifold with a concomitant slowdown of the excited state deactivation. This phenomenon was proven afterwards by means of a detailed study of the effect of the number of NHC units and the resulting photophysical properties of the corresponding Fe^{II} complexes.[17]

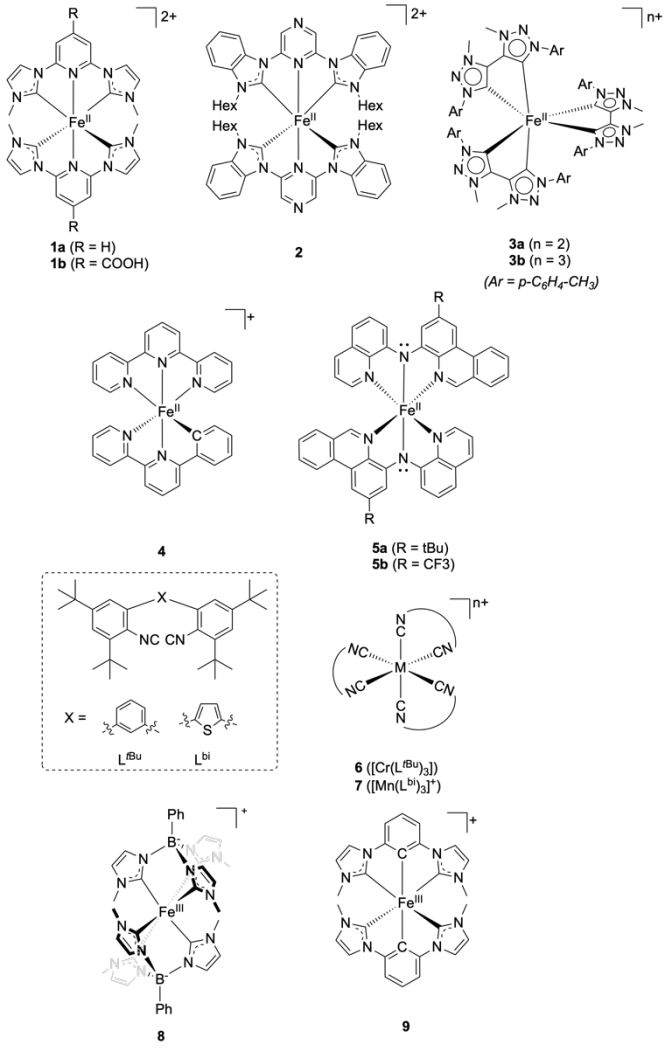

Figure 1. Selected 3d photoactive complexes based on different ligand designs. Counterion is PF_6^- for all charged compounds.

Further improvements can be achieved by modifying the electronic properties of the tridentate ligand (Figure 1). For instance, our group reported the addition of a carboxylic group on the central pyridyl ring of **1a** that almost doubled the ^{3}MLCT lifetime up to 16 ps (complex **1b**).[18] Switching from imidazolylidene (Im) to benzimidazolylidene (bIm) moieties in the ligand further increased the excited state lifetime up to 26 ps.[19] Selection of pyrazine as the central azine in combination with bIm moieties as in complex **2** resulted in the record value to date (32 ps) for tridentate ligands.[20]

The increase of the ligand-field splitting and hence the MLCT lifetime can be also achieved by reducing the angular strain around the metal centre.[21–26] This effect can be nicely illustrated by Ru^{II} complexes, where the angularly strained $[Ru(tpy)_2]^{2+}$ complex (tpy = 2,2':6',2''-terpyridine) undergoes an ultra-fast deactivation via the population of the MC states,[27] while the weakly distorted homologue $[Ru(bpy)_3]^{2+}$ (bpy = 2,2'-bipyridine)[28] avoids non-radiative deactivation channels and exhibits intense luminescence at room temperature.[29] Thus the coordination of iron with a bidentate instead of a tridentate ligand has a profound impact on the photophysics of an organometallic complex. In this regard, the introduction of bidentate bis-NHC units, namely 4,4'-bis(1,2,3-triazol-5-ylidene) (btz) ligands, in complex **3a** (Figure 1) resulted in an outstanding 528 ps ^{3}MLCT lifetime due to the presence of 6 Fe-carbene bonds within the inner coordination sphere of Fe^{II}.[30] However, it is important to point out that, in comparison with the previously reported examples, these carbenes are mesoionic.

Apart from NHC, other strong-field ligands have been explored with the aim of obtaining photoactive iron complexes. Though already investigated a few decades ago by Winkler and Sutin,[31,32] the slowdown effect on the MLCT relaxation dynamics upon using strong ligand-field cyanide ligands was not unequivocally demonstrated until recently.[26,33] Cyclometalating phenyl ligands can alternatively be used as theoretically predicted by the groups of Dixon[34] and Jakubikova[35]. Though synthetically more challenging, an air-stable cyclometalated ferrous complex **4** was successfully obtained by Bauer and co. in 2019, exhibiting a 5.5 times longer ^{3}MLCT lifetime than that of $[Fe(tpy)_2]^{2+}$ upon substituting one lateral pyridine by a phenyl unit.[36] Another remarkable example includes strong σ-donor anionic nitrogen atoms as in complexes **5** (Figure 1), where diarylamido ligands were used.[37]. These complexes exhibited panchromatic absorption features with impressive nanosecond (*ca.* 2.0–2.7 ns) excited state lifetimes. Mixing of metal-centred with ligand-centred orbitals at the HOMO level (partial 'HOMO inversion'[38]), together with the stabilisation of the ligand-centred LUMO due to the extended ligand π-conjugation may be seen as the reasons for a very low optical gap corresponding to a "$\pi_{\text{anti-bonding}}$-to-ligand charge transfer" (PALCT) transition. Computationally the ^{3}MC states were shown to be at higher energies than the PALCT state, thus well explaining these outstanding experimental results.

Unfortunately, in spite of the unprecedented long lifetimes reached for the low-lying MLCT excited states in Fe^{II} complexes, luminescence yields were not reported. However, it is worth to note that isoelectronic $3d^6$ MLCT emitters can indeed be obtained by replacing the central metal as recently reviewed.[39,40] For instance, this original approach has been successfully demonstrated very recently for Cr^0[41,42] or Mn^I.[43] Two examples are shown in Figure 1 (complexes **6**[41] and **7**[43]). In all cases, these compounds comprise chelating isocyanides ligands and result in weak room-temperature emissions (photoluminescence quantum yields up to 0.09%) in the few ns regime. As for organoferrous complexes, selection of strong-field ligands is mandatory in order to sufficiently destabilise the low-lying MC states.

Changing $3d^6$ Fe^{II} to $3d^5$ Fe^{III} leads, nevertheless, to a completely different photophysical scenario where low-lying excited states are of ligand-to-metal charge transfer (LMCT) character instead.[39] As a matter of fact, these compounds have a low-spin $^2T_2$ electron configuration in the ground state under a strong ligand field. Upon excitation, ^{2}LMCT states are populated and spin-allowed photoluminescence can become competitive over other deactivating processes if the access to $^{4/6}$MC states is not energetically favoured. This is the case for three luminescent compounds with coordination spheres comprising NHC donors (complexes **3b**[44] and **8**[45]), or a combination of NHC and cyclometallating units (complex **9**).[46] Highly interestingly, the latter exhibits a very peculiar behaviour, displaying a unique dual fluorescent emission both from the lowest-lying ^{2}LMCT (τ = 0.2 ns) and higher energy ^{2}MLCT (τ = 4.2 ns) states.

All these exciting results have thus set up a new paradigm for Earth-abundant transition-metal complexes, gathering an increasing interest of the scientific community due to the new possibilities for the development of truly sustainable photoactive materials. In the case of iron complexes, while different design strategies have been reported, more systematic studies are

missing so as to provide a clearer picture of the photophysics and photochemistry of this class of organometallic compounds, where the inherent excited state electronic structure and the structural relaxation/flexibility are intimately linked.[47,48] In this microreview we will present our recent investigations on a series of Fe^{II}-NHC complexes with bidentate ligands featuring facial and meridional isomers. Their synthesis and characterization will be described, including ultrafast transient absorption spectroscopy and Time Dependent-Density Functional Theory (TD-DFT) modelling. This contribution is thus intended to shed more light on the subtle relationship between molecular structure and electronic excited state dynamics of iron complexes by analysing the effects of bidentate ligand coordination and highlighting the impact of the *fac*/*mer* isomerism.

2. Synthesis of Fe^{II} complexes with bidentate pyridyl-NHC ligands

2.1 Precursor synthesis

In all cases, the NHC precursors were typical azolium derivatives. Very interestingly from a future application point of view, these cationic compounds were conceived from widely commercially available pyridine and imidazole derivatives, making their syntheses straightforward with good to excellent yields. The different precursors here studied are shown in Scheme 1. Precursor **L1**[49] was initially obtained to enable a direct comparison with already reported complexes from 2,6-bis(imidazolium)pyridine (Scheme 1, top).[15,18] It was prepared by reacting 2-fluoropyridine with *in-situ* generated potassium imidazolate, quaternization with iodomethane and final metathesis with potassium hexafluorophosphate.

Bearing in mind the key role of NHC in the photophysics of the final complexes, precursors **L2**–**L5** were designed to allow for a fine-tuning of the stereoelectronic properties at this unit. First, the incorporation of an additional N atom in **L2** was achieved by introducing a 1,2,4-triazole ring instead of that of imidazole on the starting 2-fluoropyridine (Scheme 1, top).[50] On the other hand, extension of the π-conjugated system of the NHC moiety has proven its beneficial effects on the excited state kinetics in tridentate-based Fe^{II} complexes.[19,20] In fact, longer ^{3}MLCT lifetimes were observed for bIm-bearing complexes as a result of a higher destabilisation of MC states due to an increased π-backbonding (*vide supra*). Therefore, these results prompted us to investigate this effect as well in bidentate ligands with the benzannulating precursor **L1**. Precursor **L3** was thus prepared as aforementioned described by selecting benzimidazolate as the nucleophilic reactant (Scheme 1, top).[51] Nevertheless, a second fusion pattern was possible at the N3–C4 instead of C4–C5 positions with respect to the parent imidazole framework, which could eventually have a non-negligible impact on the resulting complexes. In this case, imidazo[1,5-*a*]pyridinium precursors **L4** (R = H) and **L5** (R = CH_3) were prepared via a microwave-assisted stepwise cyclizing condensation reaction involving 2-aminopyridine and 2-formyl or 2-acetylpyridine, respectively (Scheme 1, bottom).[51]

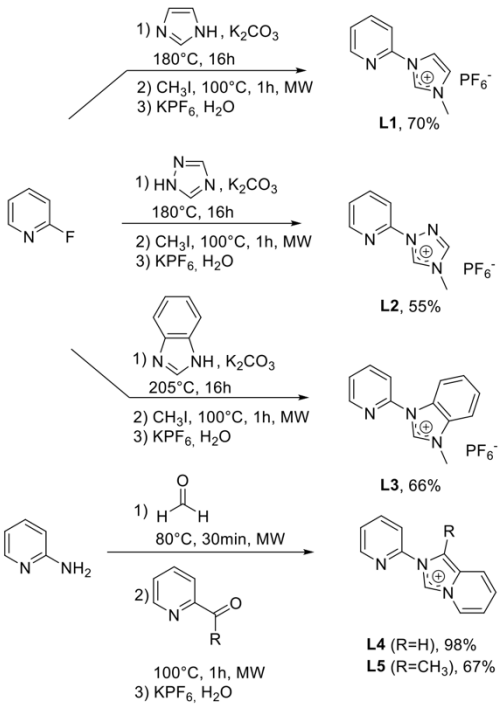

Scheme 1. Synthesis of **L1–L5** ligand precursors: (top) via a nucleophilic aromatic substitution; (bottom) via a stepwise cyclizing condensation pathway.

2.2 Synthesis of organometallic complexes

Different synthetic strategies can be employed for the complexation of NHC-based ligands, often with particular precautions against oxygen and moisture due to the extremely high reactivity of carbenes. The commonly used approach is based on the direct coordination of free carbene ligands to the iron centre, which can be performed in one-pot or stepwise reactions. The one-pot procedure is based on the direct generation of the reactive carbene species in the reaction medium in the presence of the metallic source to be coordinated to. Alternatively, the carbenic ligand can be coordinated to the metal ion in a second step. Strong bases are typically used to deprotonate the azolium moiety such as BuLi, NaH, potassium *tert*-butoxide or KHMDS, while halide salts ($FeCl_2$ or $FeBr_2$) are the most common iron(II) sources.

Moreover, softer alternatives have been also developed. More precisely, metals such as silver[52] or magnesium[53] can be used to form a metal–NHC intermediate, from which transmetalation may occur. Interestingly, these reactions can be performed at room temperature, and problems of carbene dimerization are greatly reduced.

In our case, complexation reactions were optimized using the **L1** precursor with usual Schlenk techniques following a one-pot procedure in DMF at room temperature using potassium *tert*-butoxide and iron(II) chloride as base and metallic source, respectively (Scheme 2 and Table 1).[54] The so-formed complexes were then precipitated with a saturated solution of potassium hexafluorophosphate. After purification, the target **C1** complex was obtained in 44% yield as an inseparable mixture of geometric, namely facial (*fac*) and meridional (*mer*), isomers with a 1 *fac* to 14 *mer* ratio.

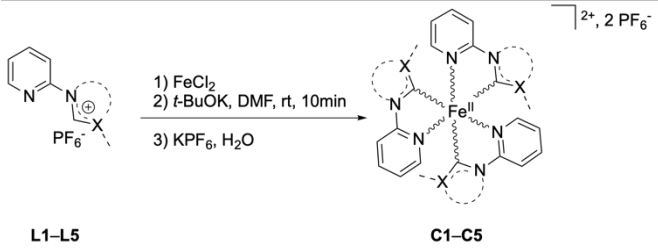

Scheme 2. Synthesis of complexes **C1**–**C5**.[49–51]

Table 1. Complexation reaction associated data.

Ligand / Complex	NHC precursor	Yield (%)	*fac*/*mer* ratio
L1 / **C1**[49]		44	1/14
L2 / **C2**[50]		22	1/8
L3 / **C3**[51]		33	1/6
L4 / **C4**[51]	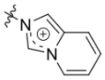	39	1/3
L5 / **C5**[51]	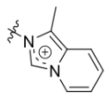	27	1/4

This complexation methodology was further extended to 1,2,4-triazole-based **L2**[50] and benzannulated **L3**–**L5**[51] precursors. The corresponding complexes **C2**–**C5** were achieved in moderate yields with different *fac* to *mer* ratios: 1/8 for **C2**,[50] 1/6 for **C3**,[51] 1/3 for **C4**[51] and 1/4 for **C5**[51] (Scheme 2 and Table 1). From these data it becomes apparent that bulkiness and steric effects may play an important role since the highest *mer* preference was obtained with the least steric demanding ligands, *i.e.* **L1** and **L2**, in spite of their rather different anticipated trans-effects,[55] while the more sterically demanding **L3**–**L5** resulted in a higher *fac* content. Additional experiments are currently ongoing in our laboratory to properly ascertain the origin of these results.

2.3 Geometry control

Besides its synthetic interest, the control of the stereoselectivity during complexations may be crucial with respect to the properties of the resulting complexes. Indeed, the geometrical differences upon facial and meridional ligand arrangements can result in distinct photophysical, electrochemical and magnetic behaviour to name a few.[56–58]

Computational investigations of the excited state properties of *fac* and *mer* isomers of **C1** (see below) revealed that the meridional isomer would display the shortest excited state lifetime. Hence, the facial isomer appeared to be the most promising one from a photophysical point of view,[49] and we turned then our attention to controlling the stereoselectivity of the facial complexes of **C1**.

To address this challenging objective, the **L1** precursor was preorganised on a triethylamine platform yielding the hemicage precursor **L6** as depicted in Scheme 3.[54] It is worth to note here the remarkable effect of microwave irradiation in its synthesis, allowing for an almost quantitative yields in only 1 h as compared with other reported structurally-related compounds requiring up to 7 days of reaction.[59] The corresponding complex **C6** was obtained following the aforementioned protocol albeit using more dilute conditions to suppress possible polymerization side-reactions.

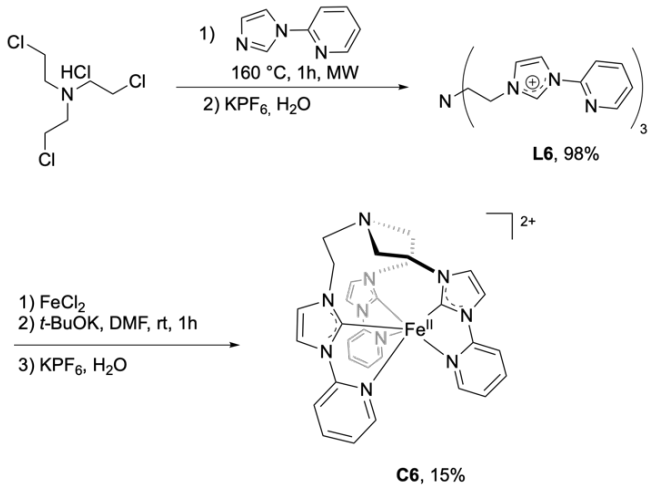

Scheme 3. Synthesis of tripodal ligand precursor **L6** and subsequent hemicaged complex **C6**. Counterion is PF_6^- for all charged compounds.

3. Absorption spectra and electrochemical properties

All complexes were characterized by UV-vis spectroscopy and electrochemistry, and the main results are shown in Table 2. The nature of the ligand around the Fe^{II} centre plays a crucial role in the specific electrochemical and optical properties. Nevertheless, all complexes showed similar general features: (i) presence of intraligand [$\pi \rightarrow \pi^*$] transitions in the UV region and appearance of two news bands in the visible range corresponding to MLCT states, the highest-energy one being attributed to iron–carbene [$d \rightarrow \pi^*_{carb}$] transitions while the lowest-energy one to iron–pyridine [$d \rightarrow \pi^*_{py}$] transitions;[60] (ii) iron-centred oxidation and ligand-centred reduction.[26,61]

3.1. Imidazolylidene-containing complexes C1 and C6

The UV-vis spectra of bidentate **C1** and **C6** are depicted in Figure 2, together with that of their tridentate counterpart **1a**[19] for the sake of comparison. Absorption profiles of both bidentate complexes appear blue-shifted with respect to **1a**. When comparing **C1** (mostly *mer* configuration) and **C6** (pure *fac* configuration), a slight red-shift (*ca.* 9 nm) is observed for the

latter along with a reduction of the intensity of the MLCT [d → π*$_{py}$] band.

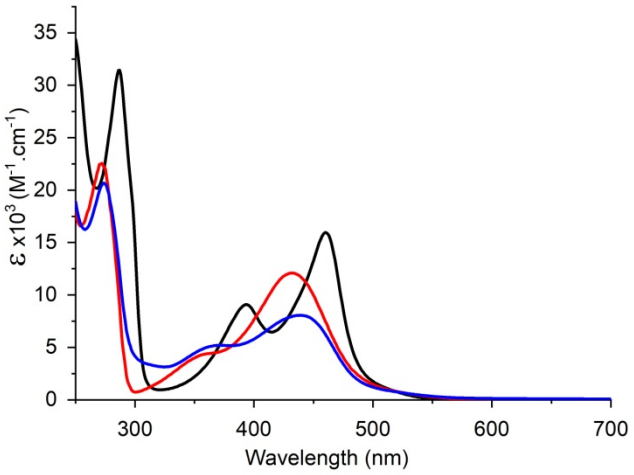

Figure 2. UV−vis spectra of **1a** (black), **C1** (red), and **C6** (blue) in air-equilibrated CH_3CN solution.

As for the electrochemical properties of **C1** and **C6**, both showed single monoelectronic anodic waves corresponding to the reversible oxidation of the iron center (Fe^{II} to Fe^{III}) at 0.67 and 0.63 V/SCE, respectively. These values are remarkably lower than that of $[Fe(bpy)_3]^{2+}$ ($E_{1/2}$= 1.05 V/SCE),[62] and can be interpreted as the result of the almost negligible π-accepting properties of the NHC respect to a pyridyl moiety. These oxidation potentials are also lower than that of tridentate **1a** ($E_{1/2}$ = 0.71 V/SCE), evidencing a higher destabilisation of the frontier t_{2g}-like orbitals that is the most pronounced in **C5** and **C6**. Nevertheless, an effect of the rigidity imposed by the tripodal ligand on the solvation and electronic properties cannot be excluded.[63]

In the negative bias, two monoelectronic peaks were observed for **C1** and **C6** at *ca.* -2.00 V/SCE. These processes can be ascribed to pyridine-localized antibonding π* orbitals. In the case of tridentate **1a**, it only showed one monoelectronic reduction wave, though at a similar potential. The irreversible nature of these electron transfers impeded a fair comparison among these complexes. However, there is no doubt about the more destabilised π* orbitals of NHC-based complexes with respect to their polypyridine analogues ($E_{1/2}$ = -1.30 V/SCE[62] for $[Fe(bpy)_3]^{2+}$ and $E_{1/2}$ = -1.20 V/SCE[64] for $[Fe(tpy)_2]^{2+}$).

Table 2. Photophysical and electrochemical data for tridentate complex **1a** and bidentate complexes **C1**–**C6**.

	$\lambda_{abs,max}$ (nm) [ε($M^{-1}.cm^{-1}$)]	$E_{1/2}(Fe^{III}/Fe^{II})$ (V/SCE)	E_{red} (V/SCE)	ΔE (eV)
1a	287 [31400] 393 [9000] 460 [15900]	0.71 (rev)	-2.00 (irrev)	2.71
C1	272 [26000] 360 [5200] 430 [12100]	0.67 (rev)	-1.88 (irrev.) -1.93 (irrev)	2.55 2.60
C2	273 [13654] 340 [4417] 410 [7980]	1.04 (rev)	-1,68 (rev)	2.74
C3	286 [60820] 337 [12700] 414 [13980]	0.87 (rev)	-1.63 (rev)	2.50
C4	271 [44000] 394 [5670] 481 [9700]	0.70 (rev)	-1.68 (rev)	2.38
C5	273 [51725] 389 [5910] 490 [12100]	0.61 (rev)	-1.66 (rev)	2.27
C6	273 [19500] 369 [4500] 438 [8000]	0.63 (rev)	-1.99 (irrev) -2.10 (irrev)	2.62 2.73

[a] Measured in CH_3CN at 25 °C. [b] First oxidation potential. Potentials are quoted *vs* SCE. Under these conditions, $E_{1/2\ (Fc+/Fc)}$ = 0.39V/SCE. Recorded in CH_3CN using $Bu_4N^+PF_6^-$ (0.1M) as supporting electrolyte at 100 mV. s^{-1}. [c] Electrochemical band gap ($\Delta E = E_{ox} - E_{red1}$)

From these results, the observed blue-shift of the absorption bands in bidentate **C1** and **C6** in comparison with tridentate **1a** can be related to a shorter ligand π-system (higher antibonding π* orbitals) since metal-based orbitals are more destabilised in **C1** and **C6**. On the other hand, it is worth noting how facial coordination allows for an enriched iron centre resulting in lower-lying MLCT transitions, albeit with a reduction of the absorption intensity, as observed for **C6** with respect to **C1**.

3.2. Modified carbenes: complexes C2–C5

Regarding complex **C2**,[50] its UV-vis spectrum is plotted in Figure 3 (top). The presence of a supplementary pyridinic nitrogen atom at the NHC moiety leads to a blue-shift (20 nm) of both MLCT bands (340 and 410 nm) with respect to those of **C1** (360 and 430 nm), while the IL band (273 nm) remains unaffected. Furthermore, the analysis of its electrochemical properties showed a reversible behaviour in both positive and negative ranges, with an oxidation potential of 1.04 V/SCE and a reduction potential of -1.68 V/SCE.

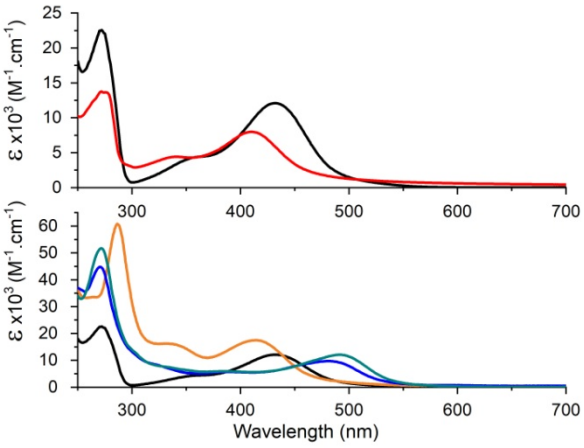

Figure 3. UV−vis spectra of **C1** (black), **C2** (red), **C3** (orange), **C4** (blue) and **C5** (green) in air-equilibrated CH_3CN solution to show: (top) heteroatom-doping effect at the NHC unit; (bottom) benzannulation effect at the NHC unit.

Complexes **C3**–**C5**, however, allow to evaluate the effect of incorporating π-extended NHC ligands.[51] The corresponding UV-vis spectra are depicted in Figure 3 (bottom). For these

compounds, the increased molar extinction coefficient of their IL bands (~275 nm) is consistent with the extension of their π-conjugated system. Although the intensity of the MLCT bands is similar for **C3**–**C5** as well as **C1**, the former clearly showed a distinct behaviour depending on the annulated ring position in comparison with non-annulated **C1**. For instance, bIm-based **C3** displays a red-shift (15 nm) of the IL band (287 nm) and a blue-shift (*ca.* 20 nm) of the MLCT bands (337 and 414 nm). As for imidazo[1,5-*a*]pyridine-3-ylidene (ImPy)-based **C4**–**C5**, only the MLCT bands (394 and 481 nm for **C4**; 389 and 490 nm for **C5**) are affected, being instead red-shifted by up to 60 nm. The small differences between **C4** and **C5** are due to the presence of a methyl substituent at the 5-membered ring in **C5**.

Electrochemical properties also changed as a function of the benzannulation. In the positive domain, oxidation potentials varied as follows: **C3** > **C4** > **C5**, with **C4** having a similar potential as **C1** and all being lower than that of **C2**. These monoelectronic transfers were reversible and associated to Fe^{II} oxidation. At negative potentials, all reductions were found to be bielectronic reversible transfers as opposed to **C1**, where two monoelectronic irreversible waves were identified. Contrary to **C1** and **C6**, the reversibility of these processes allowed the comparison between the electrochemical band gap (ΔE) and the MLCT energies, which showed the same tendency.[65]

The oxidation potentials reflect the distinct π-accepting character of the NHC units since it depends on the energy of the frontier t_{2g}-like orbital manifold. Complex **C2**, with a remarkably high oxidation potential (1.04 V/SCE), seems to be the best π-acceptor. The additional N atom in the NHC unit reduces the mesomeric donation of the adjacent N atoms into the p carbenic orbital, increasing its π-acceptance ability. In the case of **C3**–**C5**, a considerable π-accepting character could *a priori* be expected because of the competing resonance of the lone-pair at the N atoms with the carbenic p orbital and the more extended π-conjugated systems in bIm (**C3**) and ImPy (**C4** and **C5**). Considering that Im (**C1**) has low π-accepting properties, this effect is clearly observed for **C3** (0.87 V/SCE), but it is barely noticeable for **C4** (0.70 V/SCE). In the case of **C5** (0.61 V/SCE), the presence of the electron-donor methyl group results in an even higher destabilisation of the metal-centred orbitals over those of **C1** (0.67 V/SCE).

The influence of the nature of the NHC unit on the reduction potentials is less straightforward. To shed some light, the singly-occupied molecular orbitals (SOMO) for the one-electron reduced complexes have been calculated for **C1**–**C4** (Figure 4). These results showed important differences between **C1** and the **C2**–**C4** derivatives. In the former, the extra electron is located exclusively in the pyridine subsystems. In *fac*-**C1**, the electron density is distributed among the three pyridine units of the three bidentate ligands **L1**, whereas in the *mer* isomer, the electron density is delocalized over only two pyridines. In contrast, no differences are observed for *fac* and *mer* **C2**–**C4** complexes. Moreover, the extra electron is localized only over a single ligand spanning the whole aromatic system of **L2** and **L4** and only the pyridine subsystem of ligand **L3**. Therefore, the lower reduction potentials for **C2** and **C4** respect to **C1** can be attributed mostly to an increased electronic delocalisation in the reduced species, while in the case of **C3** it can be tentatively ascribed to the electron-withdrawing effect of the bIm unit on the pyridine.

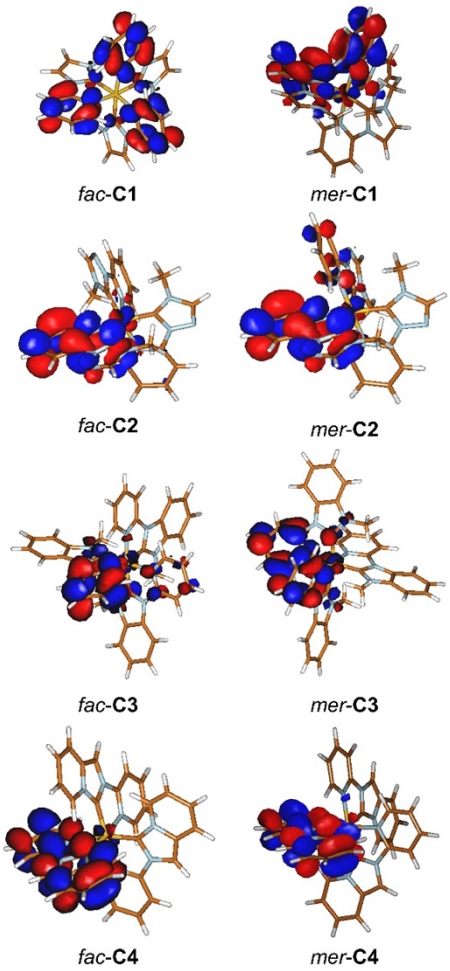

Figure 4. Singly-occupied molecular orbitals (SOMO) of the one-electron reduced **C1**-**C4** complexes. The geometries have been optimized using the unrestricted DFT/B3LYP method in combination with the 6-31+G(d,p) basis set as implemented in the Gaussian 16 software package.[66] Solvent effects (acetonitrile) have been included by means of the polarizable continuum model using the Gaussian 16 default settings.

As a consequence, the modification of the NHC unit in **C2**–**C5** improved the absorption in the UV region and lowered the reduction potentials. Nevertheless, the most noticeable effect is induced on the energy levels of the metal, which allows to rationalize their different optical behaviour as illustrated in Figure 3, where the MLCT energies are directly correlated to the π-accepting character of the selected NHC.

4. Ultrafast excited state processes

Femtosecond transient absorption spectroscopy (fs-TAS) in the near-UV/VIS spectral range was carried out on compounds **C1** to **C6**, in order to determine the relation between chemical structure (composition and configuration) and the excited state lifetimes (ESL). Except for **C2**,[50] the ESL and excited relaxation processes were reported in refs.[51,54] together with detailed simulation of the excited state potential energy surfaces (see below). As outlined in the introduction, the central question is to identify the lifetime of the ^{3}MLCT states, the population of which are in competition with the one of the ^{3}MC state. For the case of Fe^{II}-NHC complexes, with three or four carbene bonds, *i.e.* for a relatively weak ligand field splitting energies, the observed ESLs are no longer than ≈30 ps and believed to be limited by ^{3}MLCT→^{3}MC relaxation mediated

by Fe-L bond lengthening. Two simplified relaxation schemes have recently emerged, coined as “sequential” (1) and “parallel” (2):

Sequential[15,67]

$$^1MLCT^+ \xrightarrow{<100fs} {}^3MLCT^+ \xrightarrow{\tau_2} {}^3MC \xrightarrow{\tau_3} S_0 \quad (1)$$

Parallel[54]

$$^1MLCT^+ \xrightarrow{<100fs} \begin{cases} {}^3MLCT_1{}^+ \\ {}^3MLCT_2{}^+ \end{cases} \xrightarrow{\tau_1} \begin{cases} T_1 \xrightarrow{\tau_2} S_0 \\ T_2 \xrightarrow{\tau_3} S_0 \end{cases} \quad (2)$$

Optical excitation populates the ^{1}MLCT singlet states, which undergo a sub-100 fs intersystem crossing into vibrationally excited triplet ^{3}MLCT$^+$ states. The sequential scheme (1) is consistent with most experiments performed on Fe^{II} complexes with tridentate ligands, displaying a ^{3}MLCT lifetime (τ_2) on the order of 10–30 ps. Their decay goes through the ^{3}MC state, which rapidly ($\tau_3 << \tau_2$) couples with the ground state S_0. Our recent experiments on Fe^{II} complexed with bidentate ligands, **C1** and **C6,** revealed a parallel population of two excited states with distinct lifetimes (relaxation scheme 2),[54] τ_2 and τ_3, the relative population of which depends on the isomeric state of the complex (see “molecular modelling” section for more details). A similar scheme of parallel population was recently reported.[68]

More recently, femtosecond X-ray emission and scattering experiments on complex **1a** (Figure 1) showed that an ultrafast branching occurs at the ^{1}MLCT level, leading to a parallel population of both the ^{3}MC and ^{3}MLCT states, as described in the “hybrid” scheme (3) below:

Hybrid [69]

$$^1MLCT^+ \xrightarrow{<100fs} \begin{cases} {}^3MLCT^+ \xrightarrow{\tau_2} {}^3MC \xrightarrow{\tau_3} S_0 \\ {}^3MC^+ \xrightarrow{\tau_3} S_0 \end{cases} \quad (3)$$

This scenario was recently confirmed for complex **1b** (Figure 1) with femtosecond vibrational coherence spectroscopy.[70]

Note that TAS, when limited to the near-UV/VIS range, cannot unambiguously discriminate ^{3}MLCT and ^{3}MC states, as discussed for Fe^{II}[71] and experimentally shown for Ru^{II} complexes.[72] Hence, a synergy between theory and experiment is required to advance a meaningful interpretation of the TAS data and cast them in equivalent relaxation schemes. That was the case in our combined studies on **C1** and **C6**,[54] and more recently on the series of benzannulated compounds **C3**–**C5**,[51] with dominantly *mer* isomers (Table 1). For the latter, the TAS data showed two photo-induced bands with separate lifetimes τ_2 and τ_3. When analysed with global fitting and target analysis, the data were consistent with the above parallel scheme (2), but also with the following modified sequential scheme:[51]

$$^1MLCT^+ \xrightarrow{<100fs} {}^3MLCT^+ \xrightarrow{\tau_1} T_1 \xrightarrow{\tau_2} S_0^+ \xrightarrow{\tau_3} S_0 \quad (4)$$

Here, T_1 is an excited triplet state, which relaxes within τ_2= 2-3 ps into a vibrationally excited ground state S_0^+. Vibrational cooling then proceeds on a 15–20 ps time scale (τ_3), which is a common time scale for ground state intramolecular vibrational energy redistribution (IVR) in polyatomic molecules. Based on the calculations of the excited state energy level (Figure 7), however, and the similarity of them with those of **C1** and **C6,** we favoured the parallel scheme (2) for the excited state relaxation scenario.

Excited state lifetimes and relaxation of C2. As pointed out in section 3.2., the additional N in the carbene-coordinating moiety stabilizes the metal-centered t_{2g}-like frontier orbitals, as well as the ligand-centered π^*. What does that imply for the excited state lifetime, which will be determined by the interplay between ^{3}MLCT and ^{3}MC? Figure 5A shows time-resolved TAS spectra of **C2** under excitation with 50-fs pulses at 400 nm, highlighting ground state bleach (GSB, ΔOD < 0), and excited state absorption (ESA, ΔOD > 0). Note that the latter is roughly 10 times smaller than the former (break on y-axis). At early delay times ($\Delta t \leq 4$ ps), the spectral profile of the GSB shows deviations from the steady-state absorption spectrum (SSA), most importantly for $\lambda < 400$ nm, which indicates the presence of ESA in this range, but overcompensated by the dominating negative GSB. As for the other bidentate compounds, the ESA displays very prominent dynamic narrowing and blue-shifts, here on two distinct time scales. For $\Delta t \leq 1.5$ ps, the ESA evolves from a broad structureless band into an asymmetric line shape with a maximum at 480 nm (1.7 ps spectrum). At later delays, $\Delta t \geq 4$ ps, a further blue-shift occurs, with the appearance of an asymmetric ESA band whose maximum is at 460 nm, further blue-shifting with time. Consequently, there is a broad range of wavelengths, 430–480 nm, for which the signal turns over from initially GSB into ESA. The GSB amplitude at 410 nm decays by 1/e in ≈ 4 ps, and further GS recovery occurs on a ≈12–15 ps time scale.

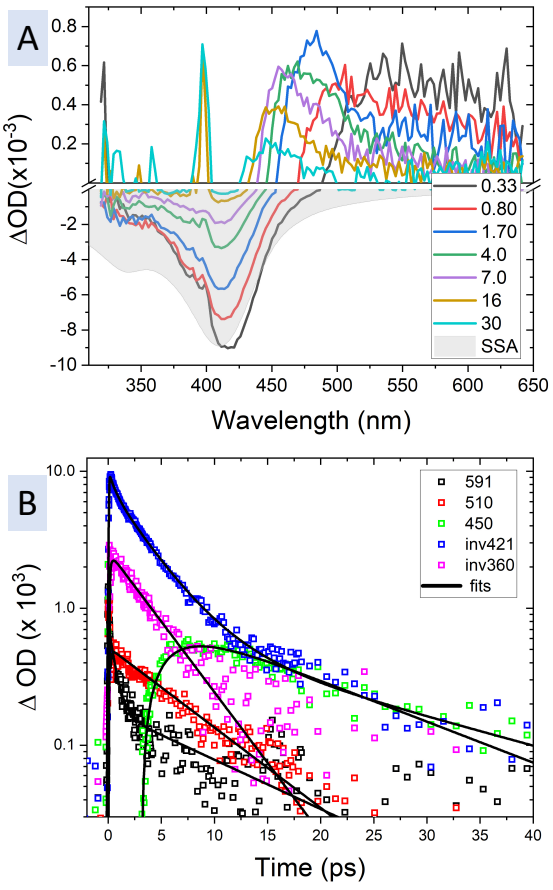

Figure 5. Transient absorption of **C2** in acetonitrile after excitation at 400 nm. A) Differential OD as a function of pump-probe delay times, between 0.33 and 30 ps (values in the legend are in ps). SSA: sign-inverted steady-state absorption spectrum. Note the different scales for the top and bottom parts of

the y-axis. Details of the dynamic spectral evolution are discussed in the text. B) Kinetic traces for wavelengths representing ESA (510 and 591 nm), GSB (sign-inverted 360 and 421 nm), and the GSB/ESA crossover at 450 nm. The slopes in the semi-log plot highlight the distinct time scales 0.3, ≈3 and 12 ps.

This is better shown by inspecting the kinetic traces at selected wavelengths (Figure 5B), together with the best fit curves obtained by 3-exponential fits. Details of the fit procedure and the obtained parameters are to be found in the Suppl. Info. From these fits, three lifetimes emerge, consistent with the above evolution of the spectra and their amplitudes, as well as with the slopes in the semi-log plot of the kinetic traces (Figure 5B): $\tau_1 \approx$ 0.2–0.3 ps, $\tau_2 \approx$ 3 ps and τ_3 = 12 ps. The results of global and target analysis are summarized in Figure 6 and in Figure S1. Despite the prominent spectral shifts, a global fit with three wavelength-independent time constants, $\sum_{i=1}^{3} A_i(\lambda)e^{-t/\tau_i}$, convoluted with a 50-fs Gaussian instrument response function, reproduces the individual kinetics very well (Figure S1). It finds τ_1 = 0.3 ps, τ_2 = 3.0 ps and τ_3 = 14 ps. The values of $A_i(\lambda)$, the DADS (decay-associated difference spectra), are consistent with the above qualitative discussion (Figure 6A). Assuming a sequential scheme of relaxation, the "evolution-associated difference spectra" (EADS) in Figure 6B are the differential spectra of the transiently populated excited states. The 0.3-ps EADS has negative amplitude at wavelengths longer than the SSA spectrum, which is indicative of stimulated emission. Hence, although significantly longer than reported for other Fe^{II} complexes,[9,73,74] we suggest this time scale to represent the lifetime of the emissive ^{1}MLCT states, or a vibrationally unrelaxed form of ^{3}MLCT. On the other hand, the 14-ps EADS is a small amplitude difference spectrum between the absorption of the 14-ps lived species and the SSA. The former is very similar to the SSA, *i.e.* it has the same shape, but is 10–20 nm red-shifted (see Figure S2). It is therefore most plausible to assign this long-lived species to the vibrationally "hot" ground state S_0^+ and to propose the excited state relaxation scheme (5) for **C2:**

$$^{1/3}MLCT^{+} \xrightarrow{\tau_1} {}^{3}MLCT \xrightarrow{\tau_2} S_0^{+} \xrightarrow{\tau_3} S_0 \qquad (5)$$

In conclusion, the excited state lifetime of **C2** is τ_2 = 3.0 ps, very similar to the value of the faster decaying excited state populations observed for the other bidentate complexes (see above). The spectral shape of the EADS of τ_2 is very similar to the those previously assigned to ^{3}MLCT states, in particular owing to the weaker but extended ESA, spanning ≈ 200 nm on the long-wavelength of the SSA spectrum.[19,20,54,75] We therefore assign this lifetime to ^{3}MLCT rather than to the ^{3}MC state. The short value is limited by intersystem crossing to S_0 probably involving ^{3}MC, which is known to act as an efficient mediator. In conclusion, despite the large stabilization of both HOMO (t_{2g}-like) and LUMO (ligand-centred) frontier orbitals as a consequence of the triazolylidene ligand (see §3.2.), the excited state quenching ^{3}MC state seems to be at lower energies than the ^{3}MLCT, and the Fe^{II}–L bond relaxation required for reaching the ^{3}MC state appears to be barrierless at room temperature. This conclusion is in line with a reduced σ-donation ability of the triazolylidene carbene.[76]

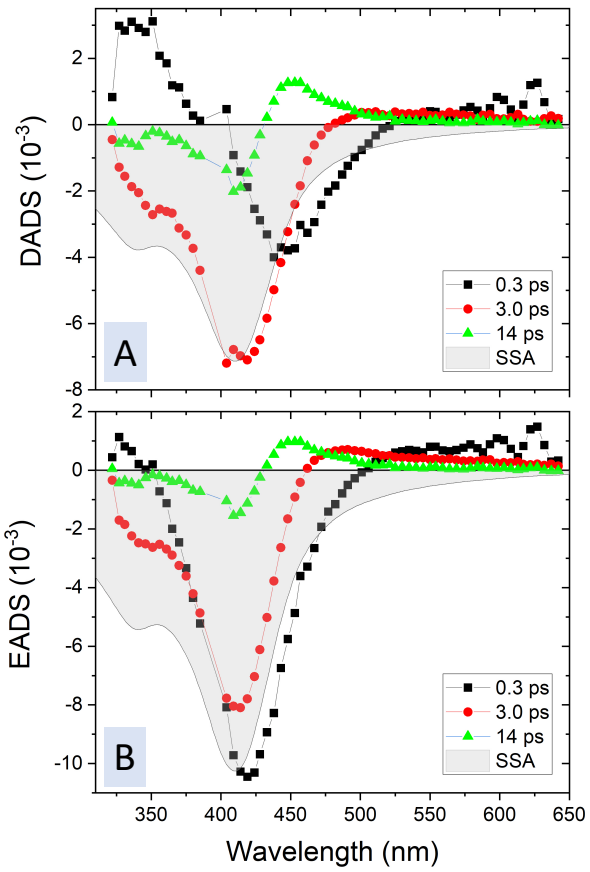

Figure 6. Results of global and target analysis of TAS data of **C2** (Figure 5). Three components are sufficient (see SI for details), and the lifetimes of 0.3, 3.0 and 14 ps are identified and differentiated by symbols (according to legend). A) Decay-associated difference spectra (DADS) associated with the three lifetimes. B) Evolution-associated difference spectra (EADS) = the differential spectra of three states involved in the excited state relaxation, assuming a sequential evolution. The assignment of the EADS to SSA: sign-inverted steady-state absorption spectrum.

5. Molecular modeling and simulation

As also evidenced by the different experimental studies reported in the previous sections, understanding, and even more controlling, the photophysics of iron-based complexes is far from standard and requires a full comprehension of the potential energy surfaces of the involved species and states. In this context, insights provided by molecular modeling and simulations have all their attractiveness and importance. Traditionally, computational methods have been used to predict structures, describe spin-crossover phenomena,[77–79] predict electrochemical properties,[80,81] rationalize optical properties,[60,82–86] and elucidate the nature and relative alignment of MLCT and MC states and the barriers for their mutual interconversion.[87,88] The large size of the iron-organic complexes often imposes the use of DFT and TD-DFT as the methods of choice for tackling this problem, although the development and use of other methodologies derived from multiconfigurational approaches (sometimes in combination with DFT, as in hybrid DFT/wavefunction formalisms) is growing in the last years.[89] On the other hand, recent advances in quantum[90–93] and surface-hopping[94,95] molecular dynamics methods have allowed[89] the simulation of the excited-state dynamics of transition metal complexes, providing a description beyond the traditional static diagrams of the excited states at relevant optimized coordinates, usually at a much higher computational cost.

If the simple localization of the energetic order between MLCT and MC states has certainly provided important hints on the electronic bases of the photophysical behaviour of iron

complexes, this strategy alone is not sufficient to account for more subtle, yet crucial, effects which may ultimately dominate the photophysics. Hence, the complete exploration of the potential energy surface landscape is fundamental to answer additional questions. Thus, the location of the energy minima should be accompanied by the determination of minimum energy path (MEP) connecting the equilibrium regions. This strategy, even if more expensive from a computational point of view, has evidenced the peculiar photophysics of bidentate NHC complexes **C1** and **C6**.[96]

Molecular modelling has been crucial in understanding the impact of the *fac*/*mer* isomerism on the photophysical outcomes of bidentate NHC–Fe^{II} complexes. Triplet MEP determinations for the two **C1** isomers have indeed shown that the ^{3}MLCT/^{3}MC internal conversions and ^{3}MC/S_0 intersystem crossings are activated by the asymmetric stretching of one Fe–N bond, hence representing a prominent route for the deactivation.[49] Highly interesting, the MLCT/MC conversions do not necessarily involve non-adiabatic transitions mediated by crossing points; instead, they proceed smoothly in an adiabatic manner. The combination of molecular modelling and TAS has identified two competitive decay channels from the lowest-lying triplet states to the ground state.[54] The fastest one involves the decay from T_2 directly to the ground state, whereas the decay from T_1 is slower due to the presence of spin-crossover regions, delaying the ground state recovery. Whereas these outcomes are difficult to verify experimentally, the synthesis of the pure *fac* **C6** has confirmed the consistence of the whole proposed mechanism.[54]

In terms of triplet PESs and electronic structure, complexes **C3**–**C5** exhibit a very similar behaviour, as documented in our recent experimental/computational study.[51] The most important singlet and triplet stationary points were characterized by means of TD-DFT, and although the PESs were not explicitly computed, the energy diagram reveals an energy positioning for **C3**–**C5** very similar to that of **C1** (Figure 7), thus pointing to a similar *fac*/*mer* influence. The similar qualitative TAS features also support this finding, even though it is important to remark that the spectroscopic analyses for **C3**–**C5** were performed on mixtures containing mostly the *mer* isomer. Consequently, the level of understanding of the role of the isomerism for these complexes is inferior to that of *mer*-**C1**[49] and **C6**[54] and therefore, a specific analysis for each isomer is lacking. In all cases, the participation of the quintet state to the relaxation has been totally excluded based on its scarce accessibility.

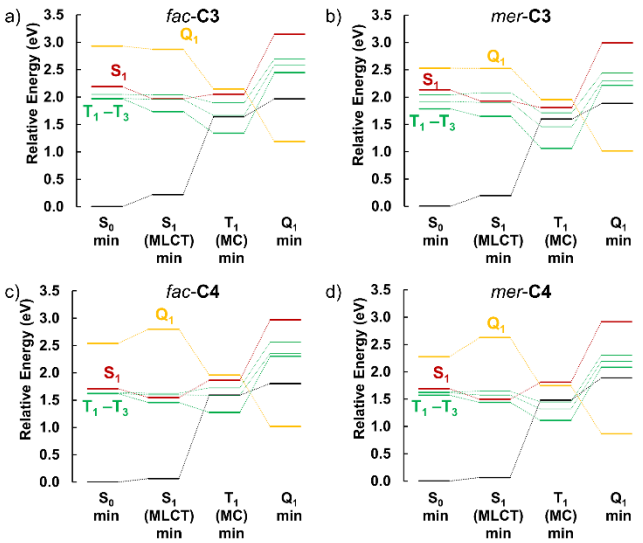

Figure 7. TD-DFT energy diagram for the *fac* and *mer* isomers of **C3** and **C4**. Only the lowest-lying singlet, triplet and quintet states are shown. Reproduced with permission from ref. [51] Copyright 2020 American Chemical Society.

The competition between the T_1 and T_2 channels, and their relative predominance, seem to depend on subtle differences in the potential energy surfaces of the two isomers, as illustrated in Figure 8 for the two isomers of **C1**. In the *fac* arrangement, the T_1 and T_2 surfaces cross in the vicinity of the Franck-Condon region, allowing for an almost equal distribution into T_2 and T_1 states. While T_2 is rather flat, T_1 is steeper and leads to a spin-crossover region that slows down the decay to S_0, as compared to the T_2/S_0 channel. Conversely, in the case of the *mer* isomer, no crossing between the T_1 and T_2 surfaces is observed at the Franck-Condon region. Hence, T_2 is in this case the most populated channel, leading to a globally fast relaxation. This work has, for the first time, pointed out the role of isomerism in dictating the overall photophysical responses in iron complexes.

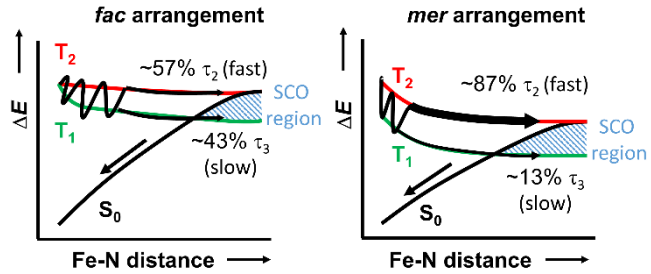

Figure 8. Schematic representation of the T_2/S_0 and T_1/S_0 pathways to deactivate the excited state in **C1**. The correspondence with the TAS components measured experimentally is also shown. Reproduced with permission from ref.[54] Copyright 2019 American Chemical Society.

Even though the chemical variety spanned by the series **C1**–**C6** reviewed here only comprises a few examples of the highly complex chemical space, one could conclude that the excited-state decay mechanism (dictated by the singlet and triplet PESs) of the *fac*/*mer* isomers are not particularly influenced by the nature of the NHC ligand, at least for this family of iron complexes. Therefore, considering the parallel relaxation scheme in these bidentate complexes, *mer* configurations result in a larger population of the excited-state decays through the faster T_2/S_0 route.

In the same spirit, the exploration of the potential energy surface of tridentate NHC complexes has revealed a different excited-state decay mechanism. Indeed, in these cases, the decay of the ^{3}MLCT state is delayed due to the presence of an energy barrier in the pathway before reaching a spin crossover region that should mediate deactivation.[20] This aspect is quite interesting and can be related to the increased overall rigidity of tridentate compounds, that is most beneficial to avoid relaxation. As a matter of fact, large scale geometrical deformations have been identified as the global coordinate driving the ^{3}MC population. As already pointed out, such a coordinate can be regarded as the asymmetric enlargement of one of the Fe–N bonds. In case of bidentate compounds, this deformation is more favourable due to the less steric constraints, hence the absence of a barrier in the potential energy surface.[96] This consideration also raises important questions. While bidentate compounds possess the ideal geometry to maximize ligand field effect and destabilize the ^{3}MC states, as compared to the ^{3}MLCT ones, this

beneficial effect is counteracted by the easier activation of the relaxing mode promoted by the higher flexibility.

More generally, these results also suggest that mostly focusing on achieving photoactive iron compounds upon modulation of the ligand field splitting is not sufficient. Instead, further attention must be also paid to maximize the metal-ligand interaction[97] as well as to rigidify the iron coordination sphere via the introduction of additional ions,[98] the presence of bulky groups at the ligand periphery[99,100] or intramolecular interactions such as π-stacking[101,102].

Molecular modelling has also recently proposed totally alternative strategies based on the functionalization of the iron complex appending a known aromatic electron acceptor, such as pyrene or phenanthrene, which could act as an energy reservoir and whose population is efficiently competing with the metal-centered relaxation.[103] This suggestion, firstly explored by Francés-Monerris et al. using computational methods, has subsequently been proven experimentally albeit on slightly different compounds.[104]

6. Conclusions/Perspectives

Almost one decade ago it was demonstrated that iron complexes could be serious candidates for the development of photoactive materials. While having been widely studied because of their spin crossover properties, this turning point for iron complexes came from a judicious design of their coordination sphere. A selection of strong field NHC-containing ligands, together with the rigidity imparted by a tridentate coordination mode, allowed for an outstanding destabilization of the metal-centered orbitals. As a result, relative long-lived MLCT states were obtained, opening a great number of new avenues for iron-based coordination compounds. In this review, we present the main strategies that have been investigated so far to achieve photoactive iron complexes, in which NHC ligands continue to play a pivotal role. Within this framework, we report some of our contributions to the field dealing with bidentate pyridine-NHC Fe^{II} complexes, from their synthesis to their ground and excited-state properties by means of combined photophysical and computational studies.

The asymmetry of the selected bidentate ligands leads to the synthesis of two distinct geometrical isomers, *i.e.* facial and meridional. Unfortunately, their physical isolation is very difficult to achieve. When compared with their tridentate congeners, absorption properties of bidentate complexes are slightly inferior. However, the excited-state lifetimes are comparable even with one less carbene unit probably due to a better metal-ligand interaction. Furthermore, we demonstrate noticeable modulations on the electronic and optical properties of these complexes upon varying the nature of the NHC moiety. Interestingly, incorporation of a π-extended NHC can have opposite effects as shown with structural isomers bIm-based **C3** and ImPy-based **C4** as a result of the strikingly different π-accepting character of the carbenes.

The approach combining TAS and computational investigations has proven instrumental for unveiling the excited state properties of these Fe^{II} complexes. Our results reveal a parallel relaxation scheme, which is in stark contrast with the sequential model followed by previous tridentate complexes. Modelling of the lowest-lying potential energy surfaces is consistent with this conclusion and identifies the asymmetric stretching of one Fe–N bond as the driving force for the deactivation. While TAS does not allow here to clearly identify the nature of the excited states, it is worth to note that computational calculations put in evidence a mixed ^{3}MLCT/^{3}MC character for the low-lying triplet states, in which the MC character adiabatically increases with Fe–N bond elongations. Furthermore, the meridional and facial ligand arrangements have a non-negligible impact on the photochemical landscapes. In fact, the relative population of each of the parallel populated excited states depends on the configuration, as demonstrated with **C1** and **C6**, with the *mer* compounds exhibiting steeper surfaces. As a result, *mer* isomers are shown to follow faster relaxation kinetics.

In spite of the great advances obtained so far,[105] we are still far from the successful development of efficient photoactive iron-based materials. In this regard, systematic studies correlating structure and properties are needed for achieving a comprehensive knowledge of the intricate photophysical and photochemical features of these compounds. As shown in this review, bidentate Fe^{II} complexes hold great promises in this area, with facial isomers being particularly more interesting as a result of their longer ESL. In addition, a higher degree of functionalisation or structural variability in case of heteroleptic complexes would be possible when compared with tridentate complexes. So which are the challenges that are currently faced? First, there is no selective synthesis either for the *fac* or *mer* isomers. Moreover, only NHC-based ligands have been studied in bidentate fashion. Last but not least, the rigidification of the coordination sphere seems to be a key player in the excited state deactivation. Therefore, the opportunities offered by bidentate ligands will surely spur further interesting developments in the near future.

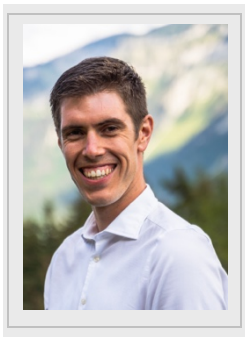

Kévin Magra received his PhD in Chemistry from the University of Lorraine (France) in 2019 under the supervision of Dr. Philippe C. Gros and Dr. Cristina Cebrián. Currently, he works as a post-doctoral researcher in the University Paris-Sud (Institut de Chimie Moléculaire et des Matériaux d'Orsay) under supervision of Dr. Marie-Laure Boillot, Pr. Talal Mallah and Pr. Fabien Miomandre. His research interests concern the design, synthesis and charaterization of various organic and organometallic compounds with applications in several fields such as light energy conversion, spin crossover properties and magnetism.

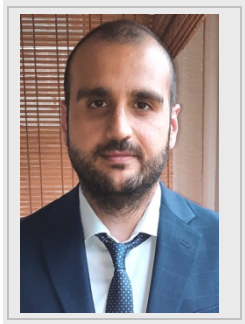

Antonio Francés Monerris received his PhD in Chemistry from the Institute of Molecular Science (University of Valencia) in 2017, supervised by Dr. Daniel Roca-Sanjuán and Prof. Manuela Merchán. From 2017 to 2020, he worked as a postdoctoral researcher at the Université de Lorraine (France), under the supervision of Dr. Antonio Monari. He currently works as a post-doctoral researcher at the Physical Chemistry Department of the University of Valencia as

a *Juan de la Cierva* fellow. His research interests span the spectroscopy and excited-state dynamics of organic and inorganic molecules, the photobiology of nucleic acids and proteins, and the molecular dynamics of biological macromolecules.

Cristina Cebrián is Lecturer at the University of Lorraine (France). She received her Ph.D. in 2011 under the supervision of Prof. A. Díaz-Ortiz and Dr. P. Prieto at the University of Castilla-La Mancha (Spain). After a post-doctoral period in the group of Prof. De Cola (2012–2013) at the Universities of Münster and Strasbourg (*Institut de Science et d'Ingénierie Supramoléculaires*), she obtained her current position in 2013. Her current research interests include the synthesis of organic and organometallic materials for optoelectronics and solar energy conversion, with special attention to sustainable synthetic approaches and challenging photoactive systems based on non-toxic and alternative metals.

Since 1st of September 2021 Antonio Monari is full professor at the Université de Paris and CNRS after having been lecturer at Université de Lorraine, Nancy since 2010. He obtained his Ph.D. from the University of Bologna in 2007 and is an expert in the use and development of molecular modelling and simulation methods for the study of photochemical and photophysical phenomena in biological systems and organometallic compounds. He also uses large scale molecular dynamics simulation, including non-adiabatic approaches, to unravel key photophysical and photobiological processes such as DNA lesion and repair, or organometallic relaxation pathways.

Stefan Haacke holds a master in Physics from the Technical University Berlin and a PhD from the University J. Fourier Grenoble (France). After a five-years assistant professorship at the Swiss Federal Institute of Technology Lausanne, with Majed Chergui, he joined the University of Strasbourg (France) as a full professor in Physics in 2004. His research team is part of the Strasbourg Institute of Physics and Chemistry of Materials (IPCMS), for which he served as the director (2013-17). As a fan of inter-disciplinary projects with chemists and biologists, Stefan's research focus is on ultrafast spectroscopy of semiconductor nanostructures, biomolecules and molecular systems for sustainable energy production, including development of femtosecond instruments. In 2017, he was chairman of the 27th Int. Conf. of Photochemistry held in Strasbourg.

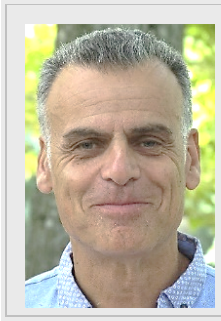

Philippe C. Gros received his PhD in Organic Chemistry from the University Claude Bernard in Lyon (France) in 1992. After a post-doctoral stay with industry, he joined the CNRS in 1994 as a Research associate. He is presently first-class CNRS Research Director in the Laboratoire Lorrain de Chimie Moléculaire (L2CM) a joint CNRS & Lorraine University unit in Nancy (France) for which he served as the director (2018-2021). His research interests encompass the development of organometallic reagents for selective functionalization of heterocycles, the design of tailor-made ligands and their transition metal complexes with applications in various fields such as energy and biology. He recently coordinated the ANR Photiron, a multidisciplinary project seeking iron complexes with long-lived excited states.

Acknowledgements

This research was funded by the French Agence Nationale de la Recherche (ANR-16-CE07-0013-02) and the European Regional Development Funds (Programme opérationnel FEDER-FSE Lorraine et Massif des Vosges 2014-2020/"Fire Light" project: "Photo-bio-active molecules and nanoparticles"), and as part of the ITI 2021-28 program of the University of Strasbourg, CNRS and Inserm, supported by IdEx Unistra (ANR 10 IDEX 0002), by the SFRI STRAT'US project (ANR 20 SFRI 0012) and EUR QMAT ANR-17-EURE-0024 under the framework of the French Investments for the Future Program. A.F.-M. is grateful to Generalitat Valenciana and the European Social Fund (project GV/2020/226) and the Ministerio de Ciencia e Innovación (project CTQ2017-87054-C2-2-P and Juan de la Cierva contract IJC2019-039297-I) for financial support. The authors would like to thank Mohamed Darari, Edoardo Domenichini, Mariachiara Pastore and Xavier Assfeld for their essential contributions to our collaborative project. We are also indebted to Fabien Lachaud and François Dupire for mass spectrometry, as well as Véronique Vaillant and Sandrine Rup-Jacques (LCP-A2MC) for NMR experiments.

Keywords: bidentate ligands • computational calculations • iron complexes • NHC • ultrafast spectroscopy

[1] O. S. Wenger, *J. Am. Chem. Soc.* **2018**, *140*, 13522–13533.
[2] H. Xu, R. Chen, Q. Sun, W. Lai, Q. Su, W. Huang, X. Liu, *Chem. Soc. Rev.* **2014**, *43*, 3259–3302.
[3] A. Hagfeldt, G. Boschloo, L. Sun, L. Kloo, H. Pettersson, *Chem. Rev.* **2010**, *110*, 6595–6663.
[4] J. Twilton, C. Le, P. Zhang, M. H. Shaw, R. W. Evans, D. W. C. MacMillan, *Nat. Rev. Chem.* **2017**, *1*, 0052.

[5] J. G. Vos, J. M. Kelly, *Dalton Trans.* **2006**, 4869–4883.

[6] M. Pastore, A. Selloni, S. Fantacci, F. De Angelis, in *First Principles Approaches to Spectroscopic Properties of Complex Materials* (Eds.: C. Di Valentin, S. Botti, M. Cococcioni), Springer Berlin Heidelberg, Berlin, Heidelberg, **2014**, pp. 1–45.

[7] S. Ferrere, B. A. Gregg, *J. Am. Chem. Soc.* **1998**, *120*, 843–844.

[8] S. Ferrere, *Chem. Mater.* **2000**, *12*, 1083–1089.

[9] G. Auböck, M. Chergui, *Nature Chem.* **2015**, *7*, 629–633.

[10] W. Zhang, R. Alonso-Mori, U. Bergmann, C. Bressler, M. Chollet, A. Galler, W. Gawelda, R. G. Hadt, R. W. Hartsock, T. Kroll, K. S. Kjær, K. Kubiček, H. T. Lemke, H. W. Liang, D. A. Meyer, M. M. Nielsen, C. Purser, J. S. Robinson, E. I. Solomon, Z. Sun, D. Sokaras, T. B. van Driel, G. Vankó, T.-C. Weng, D. Zhu, K. J. Gaffney, *Nature* **2014**, *509*, 345–348.

[11] C. Sousa, M. Llunell, A. Domingo, C. de Graaf, *Phys. Chem. Chem. Phys.* **2018**, *20*, 2351–2355.

[12] G. J. Meyer, *Inorg. Chem.* **2005**, *44*, 6852–6864.

[13] E. Jakubikova, D. N. Bowman, *Acc. Chem. Res.* **2015**, *48*, 1441–1449.

[14] Photoinduced electron transfer reactions from low-energy MC states have nevertheless been recently demonstrated. See for example P. G. Cozzi *and co., ACS Catal.* **2015**, *5*, 5927–5931 or M. D. Woodhouse and J. K. McCusker, *J. Am. Chem. Soc.* **2020**, *142*, 16229-16233.

[15] Y. Liu, T. Harlang, S. E. Canton, P. Chábera, K. Suárez-Alcántara, A. Fleckhaus, D. A. Vithanage, E. Göransson, A. Corani, R. Lomoth, V. Sundström, K. Wärnmark, *Chem. Commun.* **2013**, *49*, 6412.

[16] O. S. Wenger, *Chem. Eur. J.* **2019**, *25*, 6043–6052.

[17] P. Zimmer, L. Burkhardt, A. Friedrich, J. Steube, A. Neuba, R. Schepper, P. Müller, U. Flörke, M. Huber, S. Lochbrunner, M. Bauer, *Inorg. Chem.* **2018**, *57*, 360–373.

[18] T. Duchanois, T. Etienne, C. Cebrián, L. Liu, A. Monari, M. Beley, X. Assfeld, S. Haacke, P. C. Gros, *Eur. J. Inorg. Chem.* **2015**, 2469–2477.

[19] L. Liu, T. Duchanois, T. Etienne, A. Monari, M. Beley, X. Assfeld, S. Haacke, P. C. Gros, *Phys. Chem. Chem. Phys.* **2016**, *18*, 12550–12556.

[20] M. Darari, E. Domenichini, A. Francés-Monerris, C. Cebrián, K. Magra, M. Beley, M. Pastore, A. Monari, X. Assfeld, S. Haacke, P. C. Gros, *Dalton Trans.* **2019**, *48*, 10915–10926.

[21] M. Abrahamsson, M. Jäger, T. Österman, L. Eriksson, P. Persson, H.-C. Becker, O. Johansson, L. Hammarström, *J. Am. Chem. Soc.* **2006**, *128*, 12616–12617.

[22] Y.-Z. Hu, M. H. Wilson, R. Zong, C. Bonnefous, D. R. McMillin, R. P. Thummel, *Dalton Trans.* **2005**, 354–358.

[23] D. A. K. Vezzu, D. Ravindranathan, A. W. Garner, L. Bartolotti, M. E. Smith, P. D. Boyle, S. Huo, *Inorg. Chem.* **2011**, *50*, 8261–8273.

[24] A. K. C. Mengel, C. Förster, A. Breivogel, K. Mack, J. R. Ochsmann, F. Laquai, V. Ksenofontov, K. Heinze, *Chem. Eur. J.* **2015**, *21*, 704–714.

[25] L. L. Jamula, A. M. Brown, D. Guo, J. K. McCusker, *Inorg. Chem.* **2014**, *53*, 15–17.

[26] Y. Liu, K. S. Kjaer, L. A. Fredin, P. Chábera, T. Harlang, S. E. Canton, S. Lidin, J. Zhang, R. Lomoth, K.-E. Bergquist, P. Persson, K. Wärnmark, V. Sundström, *Chem. Eur. J.* **2015**, *21*, 3628–3639.

[27] J. P. Sauvage, J. P. Collin, J. C. Chambron, S. Guillerez, C. Coudret, V. Balzani, F. Barigelletti, L. De Cola, L. Flamigni, *Chem. Rev.* **1994**, *94*, 993–1019.

[28] S. Campagna, F. Puntoriero, F. Nastasi, G. Bergamini, V. Balzani, in *Photochemistry and Photophysics of Coordination Compounds I* (Eds.: V. Balzani, S. Campagna), Springer Berlin Heidelberg, Berlin, Heidelberg, **2007**, pp. 117–214.

[29] D. P. Rillema, D. S. Jones, *J. Chem. Soc., Chem. Commun.* **1979**, 849–851.

[30] P. Chábera, K. S. Kjaer, O. Prakash, A. Honarfar, Y. Liu, L. A. Fredin, T. C. B. Harlang, S. Lidin, J. Uhlig, V. Sundström, R. Lomoth, P. Persson, K. Wärnmark, *J. Phys. Chem. Lett.* **2018**, *9*, 459–463.

[31] J. R. Winkler, C. Creutz, N. Sutin, *J. Am. Chem. Soc.* **1987**, *109*, 3470–3471.

[32] J. R. Winkler, N. Sutin, *Inorg. Chem.* **1987**, *26*, 220–221.

[33] W. Zhang, K. S. Kjær, R. Alonso-Mori, U. Bergmann, M. Chollet, L. A. Fredin, R. G. Hadt, R. W. Hartsock, T. Harlang, T. Kroll, K. Kubiček, H. T. Lemke, H. W. Liang, Y. Liu, M. M. Nielsen, P. Persson, J. S. Robinson, E. I. Solomon, Z. Sun, D. Sokaras, T. B. van Driel, T.-C. Weng, D. Zhu, K. Wärnmark, V. Sundström, K. J. Gaffney, *Chem. Sci.* **2017**, *8*, 515–523.

[34] I. M. Dixon, F. Alary, M. Boggio-Pasqua, J.-L. Heully, *Inorg. Chem.* **2013**, *52*, 13369–13374.

[35] D. N. Bowman, A. Bondarev, S. Mukherjee, E. Jakubikova, *Inorg. Chem.* **2015**, *54*, 8786–8793.

[36] J. Steube, L. Burkhardt, A. Päpcke, J. Moll, P. Zimmer, R. Schoch, C. Wölper, K. Heinze, S. Lochbrunner, M. Bauer, *Chem. Eur. J.* **2019**, *25*, 11826–11830.

[37] J. D. Braun, I. B. Lozada, C. Kolodziej, C. Burda, K. M. E. Newman, J. van Lierop, R. L. Davis, D. E. Herbert, *Nat. Chem.* **2019**, *11*, 1144–1150.

[38] S. Mukherjee, D. E. Torres, E. Jakubikova, *Chem. Sci.* **2017**, *8*, 8115–8126.

[39] C. Förster, K. Heinze, *Chem. Soc. Rev.* **2020**, *49*, 1057–1070.

[40] C. Wegeberg, O. S. Wenger, *JACS Au* **2021**, jacsau.1c00353.

[41] L. A. Büldt, X. Guo, R. Vogel, A. Prescimone, O. S. Wenger, *J. Am. Chem. Soc.* **2017**, *139*, 985–992.

[42] C. Wegeberg, D. Häussinger, O. S. Wenger, *J. Am. Chem. Soc.* **2021**, *143*, 15800–15811.

[43] P. Herr, C. Kerzig, C. B. Larsen, D. Häussinger, O. S. Wenger, *Nat. Chem.* **2021**, *13*, 956–962.

[44] P. Chábera, Y. Liu, O. Prakash, E. Thyrhaug, A. E. Nahhas, A. Honarfar, S. Essén, L. A. Fredin, T. C. B. Harlang, K. S. Kjær, K. Handrup, F. Ericson, H. Tatsuno, K. Morgan, J. Schnadt, L. Häggström, T. Ericsson, A. Sobkowiak, S. Lidin, P. Huang, S. Styring, J. Uhlig, J. Bendix, R. Lomoth, V. Sundström, P. Persson, K. Wärnmark, *Nature* **2017**, *543*, 695–699.

[45] K. S. Kjær, N. Kaul, O. Prakash, P. Chábera, N. W. Rosemann, A. Honarfar, O. Gordivska, L. A. Fredin, K.-E. Bergquist, L. Häggström, T. Ericsson, L. Lindh, A. Yartsev, S. Styring, P. Huang, J. Uhlig, J. Bendix, D. Strand, V. Sundström, P. Persson, R. Lomoth, K. Wärnmark, *Science* **2019**, *363*, 249–253.

[46] M. Bauer, J. Steube, A. Päpcke, O. Bokareva, T. Reuter, S. Demeshko, R. Schoch, S. Hohloch, F. Meyer, K. Heinze, O. Kühn, S. Lochbrunner, *Janus-Type Dual Emission of a Cyclometalated Iron(III) Complex*, In Review, **2020**.

[47] B. C. Paulus, S. L. Adelman, L. L. Jamula, J. K. McCusker, *Nature* **2020**, *582*, 214–218.

[48] M. Darari, A. Francés-Monerris, B. Marekha, A. Doudouh, E. Wenger, A. Monari, S. Haacke, P. C. Gros, *Molecules* **2020**, *25*, 5991.

[49] A. Francés-Monerris, K. Magra, M. Darari, C. Cebrián, M. Beley, E. Domenichini, S. Haacke, M. Pastore, X. Assfeld, P. C. Gros, A. Monari, *Inorg. Chem.* **2018**, *57*, 10431–10441.

[50] K. Magra, PhD thesis, University of Lorraine (France), **2019**.

[51] K. Magra, M. Darari, E. Domenichini, A. Francés-Monerris, C. Cebrián, M. Beley, M. Pastore, A. Monari, X. Assfeld, S. Haacke, P. C. Gros, *J. Phys. Chem. C* **2020**, *124*, 18379–18389.

[52] J. C. Y. Lin, R. T. W. Huang, C. S. Lee, A. Bhattacharyya, W. S. Hwang, I. J. B. Lin, *Chem. Rev.* **2009**, *109*, 3561–3598.

[53] J. Messelberger, A. Grünwald, P. Stegner, L. Senft, F. W. Heinemann, D. Munz, *Inorganics* **2019**, *7*, 65.

[54] K. Magra, E. Domenichini, A. Francés-Monerris, C. Cebrián, M. Beley, M. Darari, M. Pastore, A. Monari, X. Assfeld, S. Haacke, P. C. Gros, *Inorg. Chem.* **2019**, *58*, 5069–5081.

[55] B. J. Coe, S. J. Glenwright, *Coord. Chem. Rev.* **2000**, *203*, 5–80.

[56] S. L. Dabb, N. C. Fletcher, *Dalton Trans.* **2015**, *44*, 4406–4422.

[57] A. B. Tamayo, B. D. Alleyne, P. I. Djurovich, S. Lamansky, I. Tsyba, N. N. Ho, R. Bau, M. E. Thompson, *J. Am. Chem. Soc.* **2003**, *125*, 7377–7387.

[58] T. Lathion, L. Guénée, C. Besnard, A. Bousseksou, C. Piguet, *Chem. Eur. J.* **2018**, *24*, 16873–16888.

[59] R. J. Soukup-Hein, J. W. Remsburg, Z. S. Breitbach, P. S. Sharma, T. Payagala, E. Wanigasekara, J. Huang, D. W. Armstrong, *Anal. Chem.* **2008**, *80*, 2612–2616.

[60] T. Duchanois, T. Etienne, M. Beley, X. Assfeld, E. A. Perpète, A. Monari, P. C. Gros, *Eur. J. Inorg. Chem.* **2014**, 3747–3753.

[61] P. S. Braterman, J. I. Song, R. D. Peacock, *Inorg. Chem.* **1992**, *31*, 555–559.

[62] D. M. Cabral, P. C. Howlett, D. R. MacFarlane, *Electrochim. Acta* **2016**, *220*, 347–353.

[63] F. Barigelletti, L. De Cola, V. Balzani, P. Belser, A. von Zelewsky, F. Vögtle, F. Ebmeyer, S. Grammenudi, *J. Am. Chem. Soc.* **1989**, *111*, 4662–4668.

[64] M. Rao, M. C. Hughes, D. J. Macero, *Inorg. Chim. Acta* **1976**, *16*, 23–236.

[65] A. Juris, V. Balzani, F. Barigelletti, S. Campagna, P. Belser, A. Vonzelewsky, *Coord. Chem. Rev.* **1988**, *84*, 85–277.

[66] Gaussian 16, Revision C.01, M. J. Frisch, G. W. Trucks, H. B. Schlegel, G. E. Scuseria, M. A. Robb, J. R. Cheeseman, G. Scalmani, V. Barone, G. A. Petersson, H. Nakatsuji, X. Li, M. Caricato, A. V. Marenich, J. Bloino, B. G. Janesko, R. Gomperts, B. Mennucci, H. P. Hratchian, J. V. Ortiz, A. F. Izmaylov, J. L. Sonnenberg, D. Williams-Young, F. Ding, F. Lipparini, F. Egidi, J. Goings, B. Peng, A. Petrone, T. Henderson, D. Ranasinghe, V. G. Zakrzewski, J. Gao, N. Rega, G. Zheng, W. Liang, M. Hada, M. Ehara, K. Toyota, R. Fukuda, J. Hasegawa, M. Ishida, T. Nakajima, Y. Honda, O. Kitao, H. Nakai, T. Vreven, K. Throssell, J. A. Montgomery, Jr., J. E. Peralta, F. Ogliaro, M. J. Bearpark, J. J. Heyd, E. N. Brothers, K. N. Kudin, V. N. Staroverov, T. A. Keith, R. Kobayashi, J. Normand, K. Raghavachari, A. P. Rendell, J. C. Burant, S. S.

Iyengar, J. Tomasi, M. Cossi, J. M. Millam, M. Klene, C. Adamo, R. Cammi, J. W. Ochterski, R. L. Martin, K. Morokuma, O. Farkas, J. B. Foresman, and D. J. Fox, Gaussian, Inc., Wallingford CT, **2016**.

[67] L. A. Fredin, M. Pápai, E. Rozsályi, G. Vankó, K. Wärnmark, V. Sundström, P. Persson, *J. Phys. Chem. Lett.* **2014**, *5*, 2066–2071.

[68] H. Tatsuno, K. S. Kjær, K. Kunnus, T. C. B. Harlang, C. Timm, M. Guo, P. Chàbera, L. A. Fredin, R. W. Hartsock, M. E. Reinhard, S. Koroidov, L. Li, A. A. Cordones, O. Gordivska, O. Prakash, Y. Liu, M. G. Laursen, E. Biasin, F. B. Hansen, P. Vester, M. Christensen, K. Haldrup, Z. Németh, D. Sárosiné Szemes, É. Bajnóczi, G. Vankó, T. B. Van Driel, R. Alonso-Mori, J. M. Glownia, S. Nelson, M. Sikorski, H. T. Lemke, D. Sokaras, S. E. Canton, A. O. Dohn, K. B. Møller, M. M. Nielsen, K. J. Gaffney, K. Wärnmark, V. Sundström, P. Persson, J. Uhlig, *Angew. Chem. Int. Ed.* **2020**, *59*, 364–372.

[69] K. Kunnus, M. Vacher, T. C. B. Harlang, K. S. Kjær, K. Haldrup, E. Biasin, T. B. van Driel, M. Pápai, P. Chabera, Y. Liu, H. Tatsuno, C. Timm, E. Källman, M. Delcey, R. W. Hartsock, M. E. Reinhard, S. Koroidov, M. G. Laursen, F. B. Hansen, P. Vester, M. Christensen, L. Sandberg, Z. Németh, D. S. Szemes, É. Bajnóczi, R. Alonso-Mori, J. M. Glownia, S. Nelson, M. Sikorski, D. Sokaras, H. T. Lemke, S. E. Canton, K. B. Møller, M. M. Nielsen, G. Vankó, K. Wärnmark, V. Sundström, P. Persson, M. Lundberg, J. Uhlig, K. J. Gaffney, *Nat. Commun.* **2020**, *11*, 634.

[70] F. Hainer, N. Alagna, A. Reddy Marri, T. J. Penfold, P. C. Gros, S. Haacke, T. Buckup, *J. Phys. Chem. Lett.* **2021**, *12*, 8560–8565.

[71] A. M. Brown, C. E. McCusker, J. K. McCusker, *Dalton Trans.* **2014**, *43*, 17635–17646.

[72] Q. Sun, S. Mosquera-Vazquez, L. M. Lawson Daku, L. Guénée, H. A. Goodwin, E. Vauthey, A. Hauser, *J. Am. Chem. Soc.* **2013**, *135*, 13660–13663.

[73] A. L. Smeigh, M. Creelman, R. A. Mathies, J. K. McCusker, *J. Am. Chem. Soc.* **2008**, *130*, 14105–14107.

[74] W. Gawelda, A. Cannizzo, V.-T. Pham, F. van Mourik, C. Bressler, M. Chergui, *J. Am. Chem. Soc.* **2007**, *129*, 8199–8206.

[75] T. Duchanois, L. Liu, M. Pastore, A. Monari, C. Cebrián, Y. Trolez, M. Darari, K. Magra, A. Francés-Monerris, E. Domenichini, M. Beley, X. Assfeld, S. Haacke, P. Gros, *Inorganics* **2018**, *6*, 63–63.

[76] H. V. Huynh, *Chem. Rev.* **2018**, *118*, 9457–9492.

[77] D. C. Ashley, E. Jakubikova, *Inorg. Chem.* **2018**, *57*, 5585–5596.

[78] I. M. Dixon, S. Rat, A. Sournia-Saquet, G. Molnár, L. Salmon, A. Bousseksou, *Inorg. Chem.* **2020**, *59*, 18402–18406.

[79] D. C. Ashley, E. Jakubikova, *Coord. Chem. Rev.* **2017**, *337*, 97–111.

[80] D. C. Ashley, S. Mukherjee, E. Jakubikova, *Dalton Trans.* **2019**, *48*, 374–378.

[81] D. C. Ashley, E. Jakubikova, *J. Photochem. Photobiol. A* **2019**, *376*, 7–11.

[82] O. S. Bokareva, O. Baig, M. J. Al-Marri, O. Kühn, L. González, *Phys. Chem. Chem. Phys.* **2020**, *22*, 27605–27616.

[83] Z. Tang, X.-Y. Chang, Q. Wan, J. Wang, C. Ma, K.-C. Law, Y. Liu, C.-M. Che, *Organometallics* **2020**, *39*, 2791–2802.

[84] L. Liu, T. Duchanois, T. Etienne, A. Monari, M. Beley, X. Assfeld, S. Haacke, P. C. Gros, *Phys. Chem. Chem. Phys.* **2016**, *18*, 12550–12556.

[85] S. Mukherjee, D. E. Torres, E. Jakubikova, *Chem. Sci.* **2017**, *8*, 8115–8126.

[86] P. Chábera, L. A. Fredin, K. S. Kjær, N. W. Rosemann, L. Lindh, O. Prakash, Y. Liu, K. Wärnmark, J. Uhlig, V. Sundström, A. Yartsev, P. Persson, *Faraday Discuss.* **2019**, *216*, 191–210.

[87] I. M. Dixon, G. Boissard, H. Whyte, F. Alary, J.-L. Heully, *Inorg. Chem.* **2016**, *55*, 5089–5091.

[88] S. B. Vittardi, R. T. Magar, B. R. Schrage, C. J. Ziegler, E. Jakubikova, J. J. Rack, *Chem. Commun.* **2021**, *57*, 4658–4661.

[89] C. Daniel, *Phys. Chem. Chem. Phys.* **2021**, *23*, 43–58.

[90] M. Pápai, T. J. Penfold, K. B. Møller, *J. Phys. Chem. C* **2016**, *120*, 17234–17241.

[91] M. Pápai, G. Vankó, T. Rozgonyi, T. J. Penfold, *J. Phys. Chem. Lett.* **2016**, *7*, 2009–2014.

[92] M. Pápai, M. Simmermacher, T. J. Penfold, K. B. Møller, T. Rozgonyi, *J. Chem. Theory Comput.* **2018**, *14*, 3967–3974.

[93] M. Pápai, T. Rozgonyi, T. J. Penfold, M. M. Nielsen, K. B. Møller, *J. Chem. Phys.* **2019**, *151*, 104307.

[94] J. P. Zobel, O. S. Bokareva, P. Zimmer, C. Wölper, M. Bauer, L. González, *Inorg. Chem.* **2020**, *59*, 14666–14678.

[95] J. P. Zobel, T. Knoll, L. González, *Chem. Sci.* **2021**, *12*, 10791–10801.

[96] A. Francés-Monerris, P. C. Gros, X. Assfeld, A. Monari, M. Pastore, *ChemPhotoChem* **2019**, *3*, 666–683.

[97] T. Reuter, A. Kruse, R. Schoch, S. Lochbrunner, M. Bauer, K. Heinze, *Chem. Commun.* **2021**, *57*, 7541–7544.

[98] B. C. Paulus, S. L. Adelman, L. L. Jamula, J. K. McCusker, *Nature* **2020**, *582*, 214–218.

[99] P. Herr, F. Glaser, L. A. Büldt, C. B. Larsen, O. S. Wenger, *J. Am. Chem. Soc.* **2019**, *141*, 14394–14402.

[100] C. E. McCusker, F. N. Castellano, *Inorg. Chem.* **2013**, *52*, 8114–8120.

[101] H. J. Bolink, E. Coronado, R. D. Costa, E. Ortí, M. Sessolo, S. Graber, K. Doyle, M. Neuburger, C. E. Housecroft, E. C. Constable, *Adv. Mater.* **2008**, *20*, 3910–3913.

[102] Y. Zhang, T. S. Lee, J. M. Favale, D. C. Leary, J. L. Petersen, G. D. Scholes, F. N. Castellano, C. Milsmann, *Nat. Chem.* **2020**, *12*, 345–352.

[103] A. Francés-Monerris, P. C. Gros, M. Pastore, X. Assfeld, A. Monari, *Theor. Chem. Acc.* **2019**, *138*, 86.

[104] P. Dierks, A. Päpcke, O. S. Bokareva, B. Altenburger, T. Reuter, K. Heinze, O. Kühn, S. Lochbrunner, M. Bauer, *Inorg. Chem.* **2020**, *59*, 14746–14761.

[105] A. Reddy Marri, E. Marchini, V. D. Cabanes, R. Argazzi, M. Pastore, S. Caramori, P. C. Gros, *J. Mater. Chem. A* **2021**, *9*, 3540–3554.